Journal of Materials Chemistry A

Accepted Manuscript

ROYAL SOCIETY OF CHEMISTRY

www.rsc.org/materialsA

Photo-Activity and Low Resistivity in N/Nb Co-doped TiO_2 Thin Films by Combinatorial AACVD.

Nicholas P. Chadwick,[1,2] Emily N. K. Glover,[1] Sanjayan Sathasivam,[1,2] Sulaiman N. Basahel,[3,4] Shaeel A. Althabaiti,[3,4] Abdulrahman O. Alyoubi,[3,4] Ivan P. Parkin[1] and Claire J. Carmalt[1]

1– Materials Research Centre, UCL Chemistry Department, 20 Gordon Street, London, WC1H 0AJ

2- Bio-Nano Consulting, The Gridiron Building, One Pancras Square, London, N1C 4AG

3 - Chemistry Department, King Abdulaziz University, Saudi Arabia

4 - Surface Chemistry and Catalytic Studies Group, King Abdulaziz University, Saudi Arabia

Abstract

A combinatorial aerosol assisted chemical vapour deposition (cAACVD) cation-anion co-doping study has been undertaken for the first time, which investigates the interplay of nitrogen and niobium co-dopants and the resultant functional properties within TiO_2 thin films. This study advantageously creates a single doped TiO_2 thin film which incorporates many compositions that transition from nitrogen doped TiO_2 to niobium doped TiO_2 across the film's width, in a single deposition. The film was split into a grid and the physical properties of each grid position characterised by X-Ray Diffraction (XRD), X-ray Photoelectron Spectroscopy (XPS), Scanning Electron Microscopy (SEM) and UV-Visible transmission spectroscopy (UV/Vis). Functional properties such as photo-catalytic activity, water contact angles and resistivity were also characterised. The study was successful in creating

and identifying the optimum dopant concentration at which these TiO_2 films exhibited both a high rate of photo-activity and favourable transparent conducting oxide (TCO) properties. Whilst most co-doping studies report relatively homogenous film, the inhomogeneity of these films allows both functional properties to exist in conjunction. To the authors knowledge this is the first instance cation and anion co-doping has been explored in the combinatorial regime.

Introduction

Titanium dioxide, particularly once doped, is a material of interest in many technological fields such as solar photovoltaics,[1] photo-catalysis[2] and transparent conducting oxides (TCOs)[3] because of its low cost, low toxicity and well defined physical properties.[4] In an effort to combine two or more functional properties, such as photo-catalytic activity and high conductivity, the use of co-dopants has featured heavily in the literature.[5–8] Usually both an anionic and a cationic dopant are incorporated; one particular set of dopants that has attracted recent interest is N/ Nb doped TiO_2. Both N doped and Nb doped TiO_2 are well characterised within the literature. Nitrogen doped TiO_2 exhibits a bandgap shift towards the visible region of the electromagnetic spectrum as well as an enhancement in UV induced photo-catalysis, which is shown to have a stoichiometric surface reaction component.[9,10] Niobium doped TiO_2 is of interest principally because of its ability to populate the Fermi level of TiO_2 closer to the conduction band, attributed to the Burnstein-Moss effect, so that Nb doped TiO_2 exhibits conductivities orders of magnitude higher than pristine TiO_2.[11–16] Whilst co-doping of this nature has been explored in powder form, thin films, which convey many advantages in terms of analysis, have yet to be studied.[20,21]

AACVD is a well understood and powerful CVD technique for the production of advanced functional materials.[19–21] The process of deposition involves a precursor which is dissolved in a suitable solvent and subsequently aerosolised. This aerosol is then passed, under inert gas flow, into the heated deposition chamber.[22] The novel combinatorial AACVD approach allows the formation of a film

which graduates from one state to another across the width of the film, perpendicular to the flow of deposition.[23,24] Each film represents many samples of differing concentrations of dopant and as such allows for the rapid screen and characterisation of many materials. Previous work has created composition gradients which change from one metal oxide through to another.[23,25]

In this work a film is created by combinatorial AACVD in which the principal dopant transitions from nitrogen to niobium across the width of the film with the change from one coinciding with another so as to create intermediate co-doped states. The film is characterised and the functional properties investigated to identify the relative concentrations of dopants that maximise functional properties such as water contact angles and photo-activity. As far as we know, this is the first time cation and anion co-doped TiO_2 samples have been synthesised in a combinatorial manner by AACVD, demonstrating that where co-doped systems are employed for future commercial applications, the relationships between dopant concentration and functional properties can be easily elucidated in an efficient manner to facilitate the creation of materials specifically suited to a particular industrial application.

Experimental

Thin film Preparation using AACVD

Nitrogen (99.99%) (BOC) was used as supplied. Depositions were obtained on SiO_2 coated float-glass. Prior to use the glass substrates were cleaned using water, isopropanol and acetone and dried in air. Glass substrates of ca. 90 mm x 45 mm x 4 mm were used. The precursors; titanium tetra-iso-propoxide (99%), niobium ethoxide (99%) and n-butylamine (96%) were obtained from Sigma-Aldrich Chemical Co. and used as supplied. Aerosols were generated in ethanol (99%) and toluene (98%) and carried into the reactor in a stream of nitrogen gas through a brass baffle to obtain a laminar flow. A graphite block, containing a Whatmann cartridge heater, was used to heat the glass substrate. The temperature of the substrate was monitored using a Pt–Rh thermocouple.

Depositions were carried out by heating the horizontal bed reactor to the required temperature of 500 ^{o}C before diverting the nitrogen line through the aerosol and hence to the reactor. At the end of the deposition, under the nitrogen flow, the glass substrate was left to cool to room temperature with the graphite block before it was removed. To synthesise the combinatorial Nb/ N co-doped TiO_2 film titanium tetra-iso-propoxide (0.5 g) and n-butylamine (3.6 ml) were dissolved in ethanol (20 ml) and added to a flask. In a separate flask was added titanium tetra-iso-propoxide (0.5 g) and niobium ethoxide (20%) dissolved in toluene (20 ml) and the separate flasks connected to a split nitrogen line with the aerosol feed leading from the individual flasks to a specially constructed baffle ensuring mixing of the individual precursor streams happened in the reactor under nitrogen flow. AACVD was carried out at 500 ^{o}C until both aerosol solutions were exhausted; effort was made to match the intensity of the aerosol so that this happened at roughly the same time.

Sample Characterisation

X-ray diffraction (XRD) was carried out using a Lynx-Eye Bruker X-ray diffractometer with a mono-chromated Cu Kα (1.5406 Å) source. X-ray photoelectron spectroscopy (XPS) was carried out using a Thermo Scientifiic K-Alpha instrument with monochromatic Al-Kα source to identify the oxidation state and chemical constituents. High resolution scans were done for the Ti (3d), Nb (3d), N (1s), O (1s) and C (1s) at a pass energy of 40 eV. The peaks were modelled using Casa XPS software with binding energies adjusted to adventitious carbon (284.5 eV). SEM images were taken on a JOEL JSM-6301F Field Emission instrument with acceleration voltage of 5 kV. Images were captured using SEMAfore software. Samples were cut into coupons representing the locations on the grid and coated with a fine layer of gold to avoid charging. The optical transmission was measured over 350–1500 nm range using a Lamda 950 UV/Vis spectrometer.

Functional Property Testing

Photo-catalytic activity was assessed using an established method based on a resazurin ‘intelligent ink’ first developed by Mills *et al.*[26] Photo induced wettability was tested by placing the samples

under a UVC lamp for 2 hours then measuring the water contact angle by placing a 5 µL droplet onto the surface of the films. The film was then irradiated overnight for 16 hours and water contact angles were re-measured. Water droplet contact angles were measured using a First Ten angstroms 1000 device with a side mounted rapid fire camera after casting a 5 µL droplet from a fixed height onto the surface. To assess the photo-catalytic activity of the film at sites marked at specific grid positions the whole sample was first washed with water, rinsed with isopropanol and irradiated for 30 minutes to clean and activate the sample. A resazurin based ink was then evenly applied using a spray gun and the photo-induced degradation of the resazurin ink monitored by ultraviolet-visible absorbance spectroscopy. Formal quantum efficiency and the formal quantum yield was then calculated. Formal quantum efficiency was calculated by dividing the rate of dye molecules destroyed per s per cm^2 by the photon flux (4.53×10^{14} photons per cm^2 per s). The formal quantum yield (FQY) was calculated by dividing the rate of dye molecules destroyed per s per cm^2 by the number of photons absorbed by the films. The photon flux and photon absorption for each film was determined using a UVX digital radiometer with a detector for 365 nm radiation attached.

Results

The combinatorial film was generated, using AACVD at a deposition temperature of 500 ^{o}C, by creating two separate N or Nb doped TiO_2 precursor solutions for the formation of nitrogen and niobium doped TiO_2 respectively. This ensured the combinatorial nature of the film. Both precursor solutions were aerosolised and fed into the deposition chamber under inert gas flow separately, utilizing a custom baffle that ensured the precursor streams mixed only when inside the reactor (Figure 1).

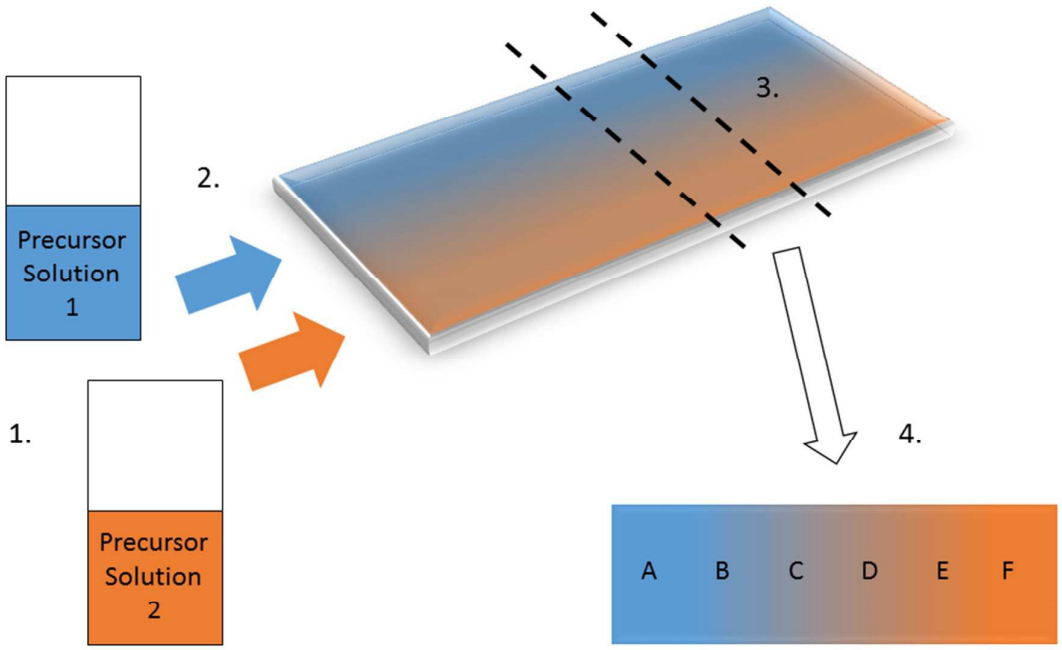

Figure 1: Two different precursors for the growth of two different oxides were dissolved (1.). The solutions were aerosolised and passed into the deposition chamber and only mix when in the chamber (2.) whereby a film was created which graduates from one material to another across its width (3.). A grid can be applied so that each position can be characterised and thus the gradual change in composition can be mapped. Each grid position represents a material with a specific level of doping thus the method is excellent at creating several doped oxides at once (4).

Once the deposition was completed the combinatorial film generated was over laid with a grid so that individual areas of the film could be selected and analysed. In this way data on how crystal structure, elemental composition and functional properties change as a result of relative concentrations of dopants was collected. The resulting film with overlaid grid can be seen in Figure 2. The graduation from yellow to aquamarine to blue to purple can be seen across the width of the film, confirming on a qualitative level that the concentration of dopants changes across its width.

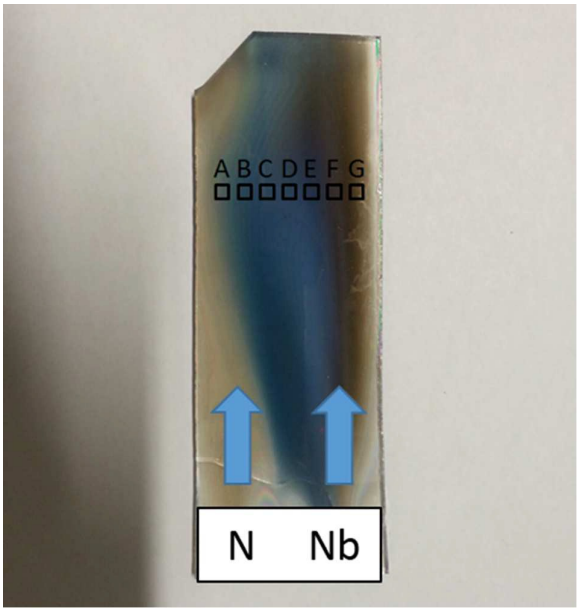

Figure 2: The combinatorial film. The left hand side is nitrogen dominant and the right hand side niobium dominant. A grid is overlaid to standardise analysis areas and create samples. The graduating nature of the film is evident with a transition from yellow to blue through to purple and eventually brown is clearly visible. The positions examined were chosen because they exhibited the smoothest progression of colour change, indicative of dopant variation, allowing meaningful analysis of changing dopant levels.

Characterisation

The combinatorial film was analysed by X-ray diffraction (XRD), X-ray photoelectron spectroscopy (XPS), scanning electron microscopy (SEM) and transmission UV/Visible spectroscopy. This allowed changes in crystallinity, elemental composition, morphology and band gaps to be charted relative to each other.

X-ray Diffraction (XRD)

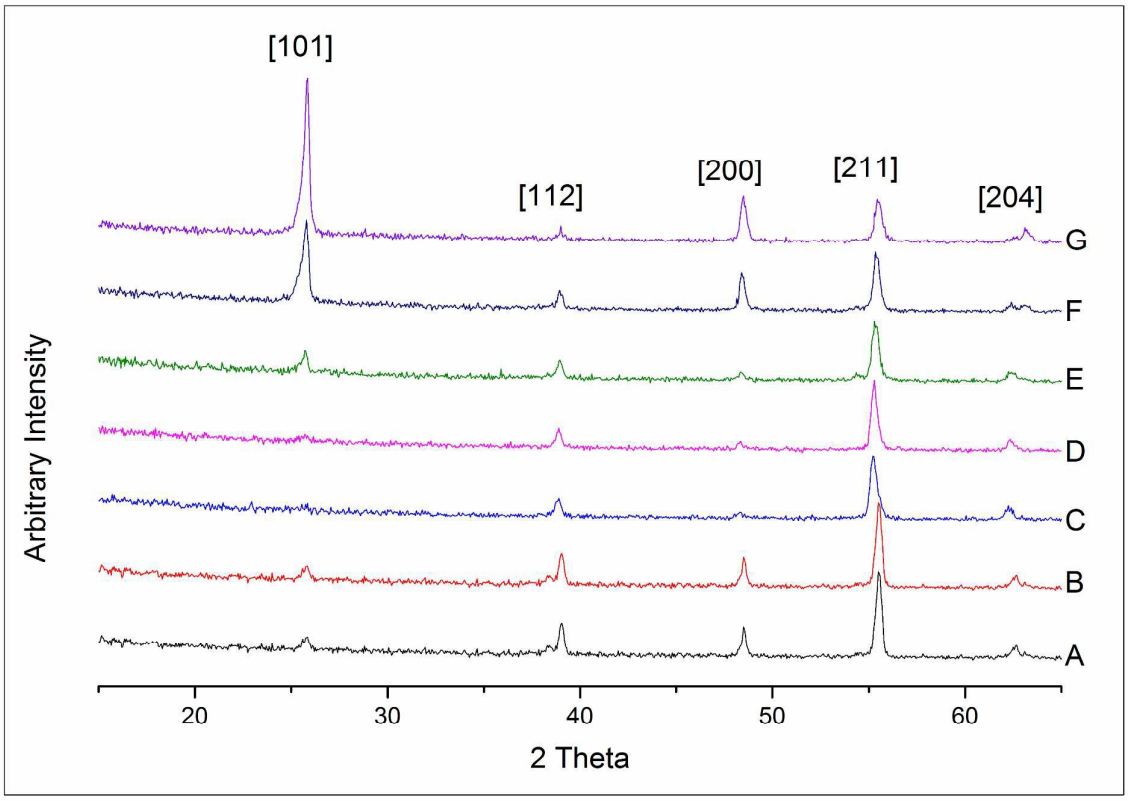

Figure 3: A graph comparing the XRD pattern from all samples A – G grown at 500 °C by combinatorial AACVD. All samples are seen to exhibit crystal structure concordant with anatase TiO_2. A change in the prevalence of peaks and shifting is evident across the samples. A change in intensity is particularly acute in the [101] and [200] planes. The [112] and [211] planes exhibit little change in intensity, however the [211] exhibits a shift in its 2Θ value as focus moves from left to right across the width of the film.

X-ray diffraction was undertaken for all samples A-G (Figure 3). All samples exhibit TiO_2 XRD reflections consistent with anatase TiO_2. No reflections were attributed to Nb_2O_5 or TiN. The prevalence of certain crystal planes is seen to fluctuate across all grid positions. All grid positions therefore display some form of preferred orientation. The [101] plane was observed to disappear from samples A – D and then reappear with heightened prevalence from samples E – G with the [200] plane changing in a similar way. The [112] plane was observed to remain constant throughout all samples as was the [211]. In the context of N and Nb doping, it is expected that Nb doped samples would exhibit a shift to lower 2θ values as seen in the [211] peak.[27] Nitrogen doping on its

own does not historically produce a lattice expansion within the TiO_2 matrix as its ionic radii is not big enough to cause this, acting either as a substitutional or interstitial dopant. Therefore any shift seen is most likely due to the uptake of Nb into substitutional positions replacing Ti^{4+} with Nb^{5+}. However given the ionic radii of Nb^{5+} (0.64 Å) and its similar size to Ti^{4+} (0.61 Å) the lack of shift in any other peak is unsurprising.

X-ray Photoelectron Spectroscopy (XPS)

High resolution XPS was used to identify the relative concentration of elements, quantifying the variances in nitrogen and niobium doping that occur across the film between positions A - G. Oxidation state and environment of both dopants were determined by comparing shifts and features of the core level spectra. Depth profiling, using Ar^+ ion sputtering, allowed for the comparison of the identity and ratios of elements at and under the surface.

Niobium was not detected at the surface though nitrogen in the form of NH_x, N_2 and NO_x was observed at all positions.[10] After 900s of Ar^+ sputtering, niobium was found to reside at positions D-G. All positions A - G exhibited peaks characteristic of Ti^{4+} at ~464.5 eV and ~458 eV for the Ti^{4+} 2p 1/2 and 3/2 peaks respectively, which is indicative of TiO_2.[28–30] This was corroborated further by the identification of O1s peaks at ~530 eV in all spectra, characteristic of oxygen in TiO_2.

Depth profile spectra were obtained at intervals of 100s of Ar^+ sputtering. Niobium was observed within the bulk from 900s of sputtering onwards. After which niobium and nitrogen levels were found to remain constant, as such Figure 4 details the concentrations of Nb and N after 900s of sputtering. Nitrogen and niobium concentration varied across the width of the film. Nitrogen concentration remained relatively constant across the film within the bulk whilst niobium was found to be more concentrated at the side where the niobium precursor entered the reactor. The variances in nitrogen and niobium doping were quantified and compared (Figure 4).

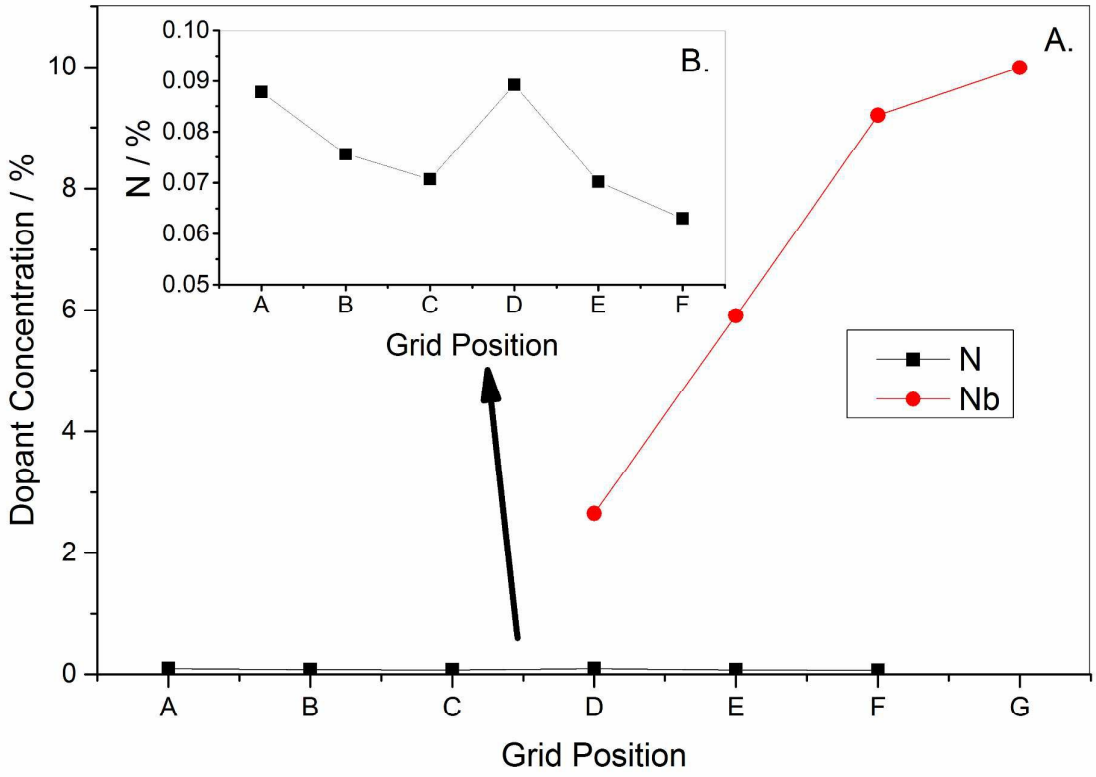

Figure 4: A. A graph comparing how the nitrogen and niobium concentration changes from positions A – G of the combinatorial film within the bulk. This was achieved by Ar^+ sputtering for 900s. Nitrogen is seen to remain constant around 0.08 (atom) % across all positions. Niobium concentration is seen to increase from around 2.6% at position C in a proportional manner to about 8% at position G. The method of combinatorial deposition to create many samples which exhibit different levels of co-doping is thus proved. All percentages calculated from XPS. B. Close up of the bulk nitrogen dopant concentration demonstrates an overall decrease from position A-G, with an increase in nitrogen concentration occurring between C-D. This can be explained by computational reports demonstrating that Nb incorporation, seen from position D onwards, favour the incorporation of substitutional nitrogen into the TiO_2 lattice.

Nitrogen was found to reside as both an interstitial (~396 eV) and substitutional (~399 eV) dopant from the surface all the way through to the bulk.[31–34] The surface concentration of nitrogen can be found in Figure 5. The concentration of nitrogen is found to vary by an order of magnitude between the surface and within the bulk were niobium is found.

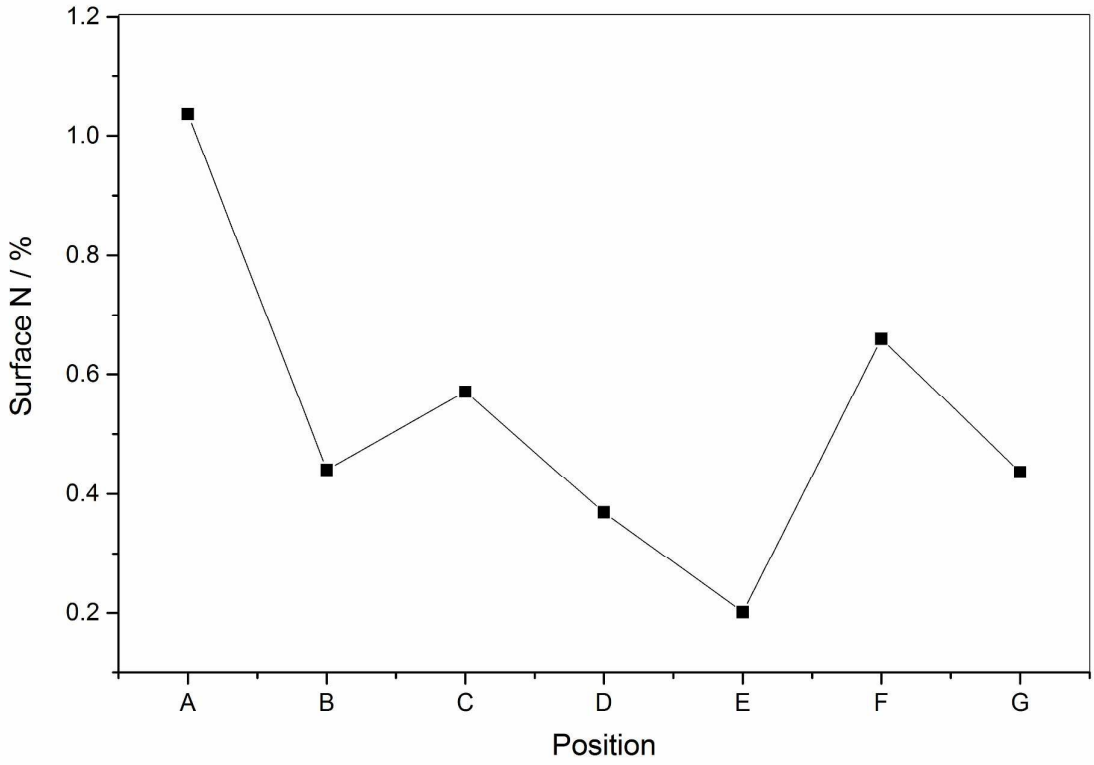

Figure 5: Surface concentration of nitrogen from position A-G. An overall decrease was observed from position A-G.

Niobium was found not to reside at the surface and only existed as a substitutional dopant deep within the bulk. Given that the process of bombardment with Ar^+ to create a depth profile is known to cause the reduction of atomic species from one oxidation state to another it is impossible to determine quantitative and meaningful levels of Nb-N bonding environments within the bulk using XPS.[35–38] This is a common issue with analysis of Nb_2O_5, TiO_2 and Ta_2O_5.[39–41] In light of conductivity values discussed later and the observation in samples D-G of peaks for Nb^{5+} at ~207 eV and ~209 eV (for $3d_{5/2}$ and $3d_{3/2}$ respectively), it is highly likely that Nb^{5+} is the dominant oxidation state within the bulk, congruent with previously reported literature.[11,13,42,12]

Scanning Electron Microscopy (SEM)

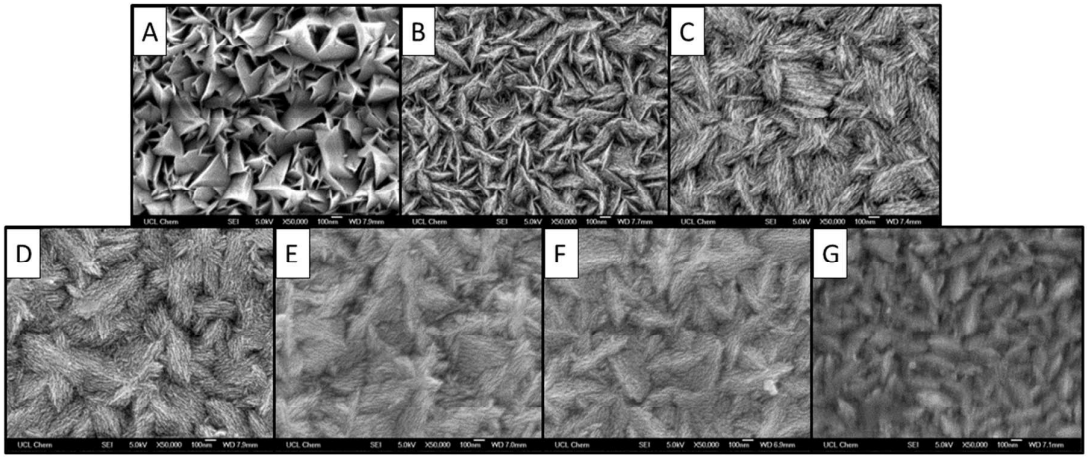

Figure 6: SEMs for positions A-G. Position A exhibits a highly porous and well defined 'shark tooth' morphology. From positions B-G there are two marked changes, overall the highly structured morphology seen in A is observed to degrade incrementally from B through to G. Also the structure appears to break down into small strands or fibres as from position A-G. All images taken at a magnification of X50,000.

SEM was taken of all samples (Figure 6). Surface morphology is an important consideration when discussing photo-catalytic rates as surface area can change as a result of variations in morphology. Differences in morphology are also responsible for fluctuations in water contact angles and other properties. The morphology seen at position A exhibits thin 'shark tooth' like growths. The film was observed to be highly porous with a high surface area. Position B exhibited very similar morphologies but the porosity was seen to decrease with the grains sitting closer to each other. The grains also exhibited secondary structure that manifested itself as veins or threads along its length. Position C exhibited a transition in morphology, with the primary 'sharktooth' structure starting to break down and the secondary thread structure starting to take over with more and more threads becoming evident. This trend continues through positions D – G until in F and G there is little left of the 'sharktooth' morphology and the threads that grew from them become the dominant morphology. Thus overall the quality of morphology was observed to decrease from left to right across the width of the film.

UV/Vis Transmission Spectroscopy

Ultraviolet- Visible transmission spectroscopy was undertaken to calculate how the bandgap changes between samples A-G (Figure 7). Bandgap values were calculated using tauc plots which utilised ultraviolet-visible spectroscopic measurements.[43] As sample A should exhibit the highest levels of nitrogen dopant and the lowest levels of niobium doping it can be, relative to the rest of the samples, considered the most similar to purely nitrogen doped TiO_2. This was reflected in the calculated bandgap at position A, which was 2.44 eV. This is concordant with much of the literature regarding nitrogen doped TiO_2. From position A through to position G the bandgap was seen to increase to and beyond the literature bandgap value for non-doped anatase TiO_2 (3.2 eV). The bandgap was seen to plateau around 3.5 eV between positions D-G. This increase of bandgap values was indicative of Nb doped TiO_2.[44,45] This increase is concordant with the observation of an elevation of bandgap in Nb doped TiO_2 with a percentage of more than 5% (E-G) caused by the Burnstein-Moss effect.[11]

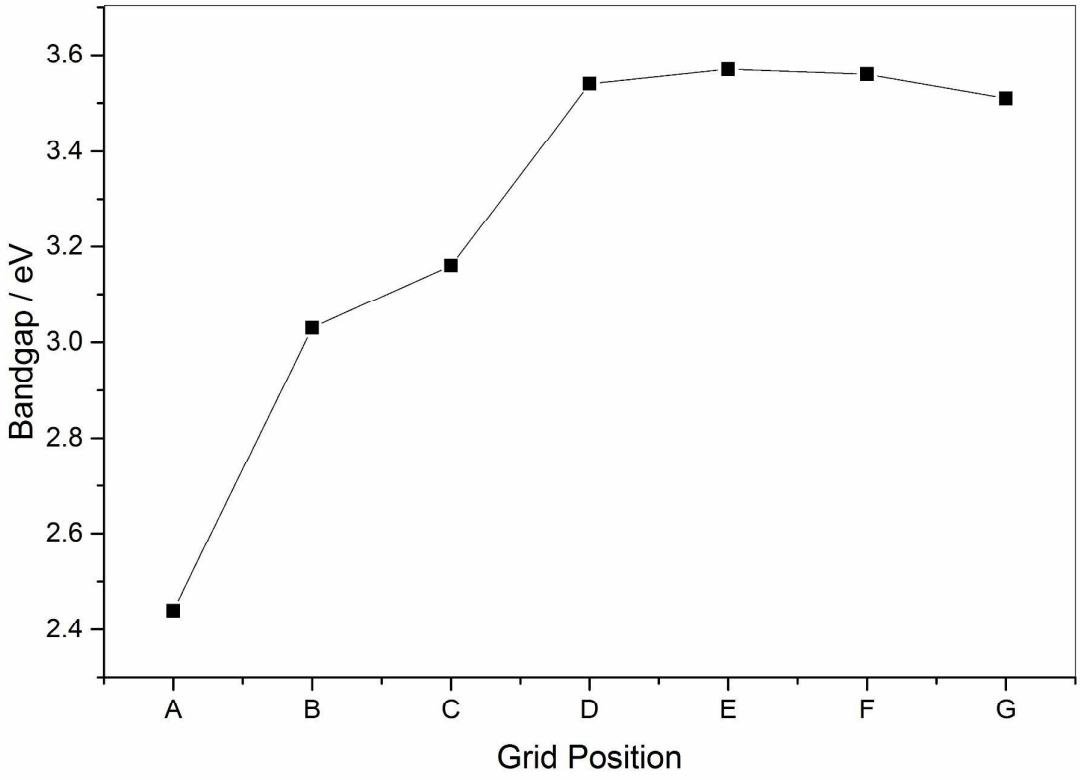

Figure 7: A graph of bandgap values for all positions A-G. At position A, which should exhibit bandgap values similar to nitrogen doped TiO_2 and a value of 2.44 eV is seen which agrees with literature published on N doped TiO_2. The bandgap is then seen to increase to 3.03 and 3.16 for position B and C respectively. This is close to the reported value of 3.2 eV for pristine anatase TiO_2. The band gap then increases past this point at position D to 3.51 eV and plateaus around 3.55 eV for positions E-G.

Transmission data was obtained which provides an idea as to the suitability of a material for use in a TCO applications (Figure S1). This can be found in the ESI. The films are found to exhibit relatively poor transmission, however this observation is tempered by the large film thicknesses measured, which are alluded to in Table 1 for positions C-G.

Functional Properties

Functional property testing was undertaken so that changes in photo-catalysis, water contact angle and resistivity that occur across the width of the combinatorial film can be correlated with changes in elemental composition, crystal structure and morphology as seen in previous combinatorial studies.[25]

Hall Effect Measurements

Hall Effect measurements were carried out for all positions. Grid position C-F provided meaningful data whilst positions A-B and G exhibited resistivity values too high to obtain data. Thin film thickness was first calculated utilising the Swanepoel method.[46] This was then used to allow the calculation of bulk carrier concentration, carrier mobility and resistivity (Table 1). It was observed that the sign of the bulk carrier concentration switched from positive to negative from position C to position D-F. This signals a change from a p-type to n-type semiconductor and is congruent with previous literature reports. The combinatorial deposition regime therefore enables the transition from p-type to n-type conductivity to be explored. The switch coincides with the appearance of Nb doping in position D to G onwards. No Nb was found at position C and as such it is only nitrogen doped explaining the p-type behaviour. Resistivity values from C-F were seen to decrease by an order of magnitude as niobium content, as seen by XPS, increases. Thus it is evident that niobium is

contributing electrons to the Fermi level and populating the conduction band with a higher proportion of mobile electrons congruent with literature reports. Whilst bulk carrier concentrations and carrier mobility were seen to vary in magnitude it is difficult to relate this to dopant effects as film thickness was seen to decrease from positions C-F, which is an artefact of the combinatorial deposition process. Given that resistivity decreased in line with a decrease in thin film thickness, it can be assumed that dopant effects are responsible for this change in resistivity across positions C-F.

Table 1: Hall Effect data for positions C-F. Thin Film Thickness is seen to vary across the width of the film which is expected as an artefact of the combinatorial deposition regime. Bulk carrier concentration is seen to switch from C to D-F from p-type (N: TiO_2) to n-type (Nb: N: TiO_2). Resistivity is also seen to decrease from C through to F which correlates with increasing niobium content seen in XPS.

Samples	Film Thickness/ nm	Bulk Carrrier Concentration/ cm^3	Carrier Mobility / cm^2 Vs^{-1}	Resitivity / Ω cm
C	1500	1.19×10^{-20}	6.49	8.06×10^{-3}
D	1379	-4.52×10^{19}	1.85×10^{1}	7.47×10^{-3}
E	494	-2.89×10^{20}	6.98	3.10×10^{-3}
F	572	-1.01×10^{19}	2.95×10^{1}	2.10×10^{-2}

Photo-catalysis

The photo-activity of all positions was measured by charting the reduction of a resazurin based ink to resorufin by UVA light (365nm), first utilised by Mills *et al* (Figure 8).[26] It was found that positions A and B exhibit the highest rate of photo-activity. From this point it was observed that photo-activity for other positions decreases incrementally from points B-G by roughly an order of magnitude. In comparison with SEM, it is interesting that the morphology observed in A and B was seen to degrade and change from point C-G. Thus morphology can be said to play a vital part in the observed rate of photo-catalysis. As the morphology seen from C-F in SEM does not change between these points, yet photo-activity was seen to continue to decrease in an incremental and proportional manner, it can be deduced that whilst morphology plays an important role in the observed rate of photo-catalysis, the role of co-dopant concentration is hinted at by the disparity between the declining photo-

catalytic rate observed from B-G and the change in morphology that occurs between B-C. Formal Quantum Yield (no. of molecules destroyed per incident photon) and Formal Quantum Efficiency (no. of molecules destroyed per absorbed photon) values were seen to mirror the photo-catalytic rate at each position (Figure 9). Position G is a more efficient photo-catalyst compared to position A as its FQY and FQE are relatively similar, whereas there is a larger disparity between the FQE and FQY at position A. This however does not take into consideration changes in surface morphology which are seen to occur from positions A to G.

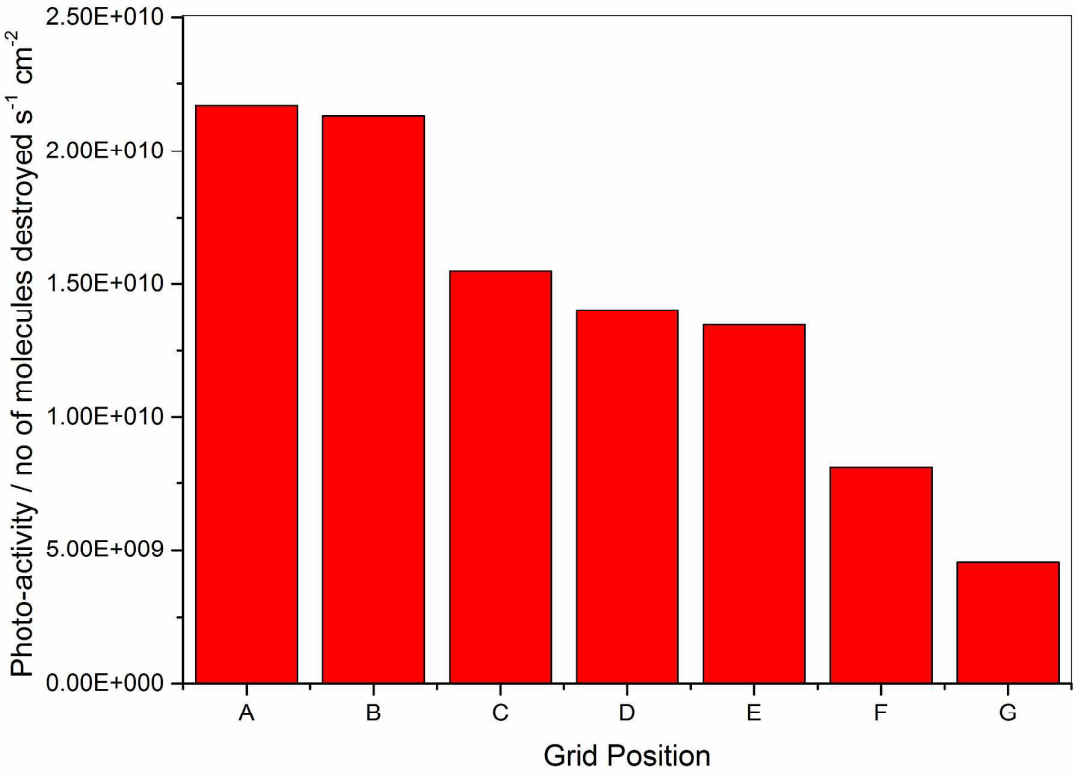

Figure 8: A graph comparing the photo-catalytic activity of all positions A–G. It was observed that UV photo-activity was highest at position A, where the level of nitrogen doping is highest and the level of niobium doping is lowest. Photo-activity proceeds to then decrease incrementally from position B – G by roughly an order of magnitude.

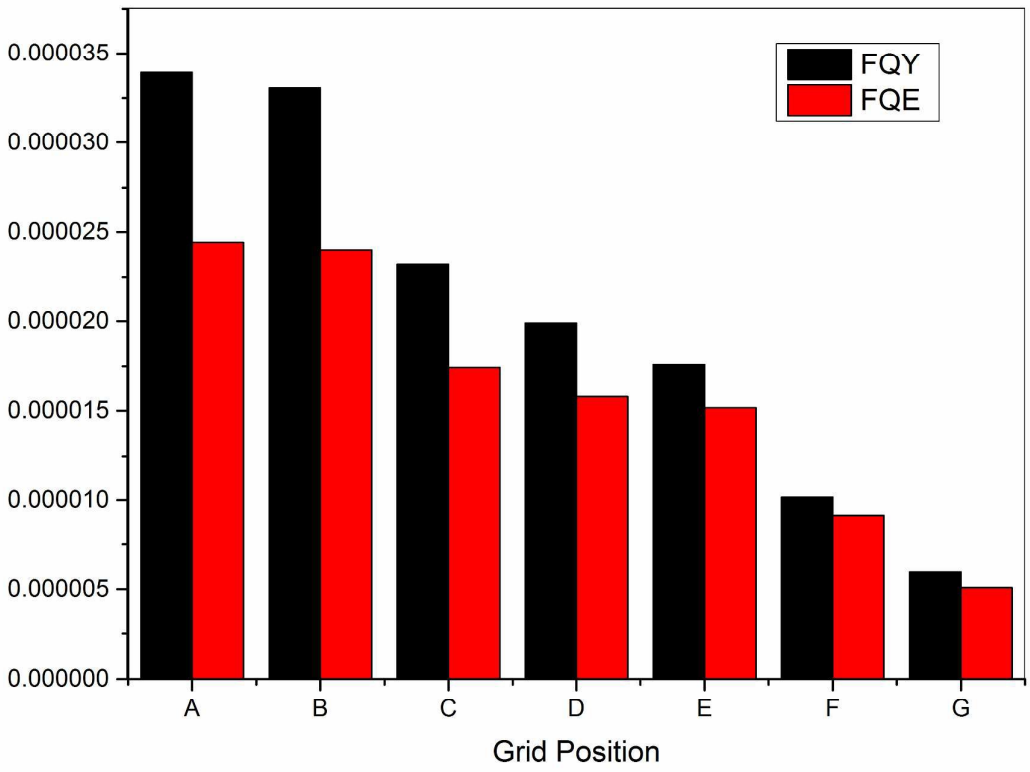

Figure 9: Formal Quantum Yields and Formal Quantum Efficiencies for all positions. A decrease in both FQY and FQE was seen as focus moves from position A to G. This mirrors the photo-catalytic rates in charting a decrease from nitrogen doping to niobium doping, which is expected. The sample at positon G is a more efficient photo-catalyst compared to position A but exhibits an overall lower rate of charge carrier generation. This does not take into account the effects that surface morphology can have, as surface morphology is seen to change across the film from positions A to G.

Water Contact Angles

Water contact angles were found to be hydrophilic at point A and then increase as focus transitions to point B. The rest of the film exhibit little change in pre-irradiation water contact angles from this point onwards with points C – G exhibiting fairly similar contact angles. After irradiation all samples were seen to exhibit photo-induced wettability, indicating that all samples were photoactive with point B exhibiting the biggest change in contact angle (Figure 10 and Table 2).

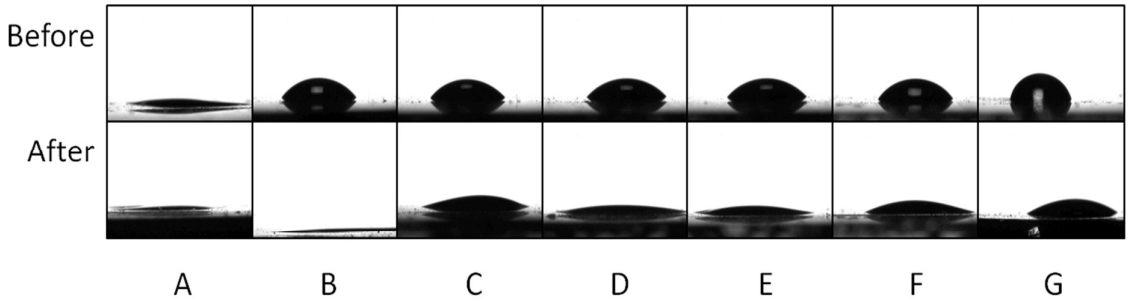

Figure 10: Water contact angles before and after 24 hours of irradiation with a 365 nm UV light source. Point A is seen to display hydrophilic behaviour both before and after irradiation. All other samples exhibit higher water contact angles, with roughly similar angles from point B – G. After irradiation all samples are seen to exhibit photo-induced wettability, with point B exhibiting the biggest change in water contact angle.

Table 2: A table of water contact data for the combinatorial film for all points A- G

Sample	**Water Contact Angle/ °**	
	Before	After
A	19.1	7.3
B	58.3	6.4
C	53.1	23.8
D	49.6	9.2
E	51.8	11.5
F	62.7	17.3
G	82.4	36.2

Discussion

XRD shows that crystalline samples of anatase TiO_2 were present across the entire width of the combinatorial film. The change in intensity of peaks, and therefore preferential orientation, in the diffraction patterns between samples demonstrates that the formation of these materials is subject to different conditions which can be attributed to the incorporation of dopants within the TiO_2 matrix. Coupled with SEM this corroborates the idea of changing preferential orientation as

microstructure was seen to change in a linear fashion from one morphology to another as the concentration of niobium changes relative to nitrogen.

XPS quantitatively confirms that nitrogen and niobium co-doped TiO_2 thin films have been synthesised. Interestingly nitrogen concentration remained relatively constant across the entire width of the film while niobium exhibited the expected tail off as focus moves from the right, where the niobium dopant stream enters the reactor, to the left. Therefore, the nitrogen is either equalising throughout the whole film by thermal diffusion in the film or n-butylamine has a longer residence time within the reactor and is diffusing into the niobium stream before deposition. Given literature reports of nitrogen thermal diffusion at 400 K and above it is possible that this is the cause of the observed homogenous N-doping, since the deposition temperature for this film is 700K.[47] However further experimentation is required to elucidate the true mechanism behind this.

Bandgap values expected for nitrogen doped TiO_2 and niobium doped TiO_2 were observed in the expected positions (A for N-TiO_2 and G for Nb-TiO_2) with a transition in between. There is no apparent lowering of the bandgap seen in literature reports for other N/Nb co-doped TiO_2 systems and this is attributed to low concentrations of nitrogen and relative inhomogeneity of the films. [17,48,49]

Regarding functional properties photo-catalysis exhibits the expected change in photo-catalysis shown in the literature with a decrease in ultraviolet photo-catalytic rate seen from nitrogen doped TiO_2 to niobium doped TiO_2. Formal quantum efficiency and yield (FQE and FQY) values were seen to mirror changes in photo-catalytic rate. That a change in morphology is concurrently seen with this transition highlights the importance of microstructure and its ability to produce an enhanced observable rate of photo-catalysis whilst the material inherently produces the same amount of charge carriers regardless of doping. When considering the contribution that dopants make to the photo-catalytic rate, it must be remembered that niobium states seen from position D-G lie within the bulk and hence contribute very little to changes in charge carrier generation or recombination

for photo-catalysis as the underlying recombination rate of TiO_2 ensures that only charge carriers generated at or near the surface undergo surface redox reactions. As the concentration of nitrogen is found to be roughly equal at all positions the decrease in photo-catalytic rate seen from positions A - G can be considered to simply arise from the transition in microstructure. Photo induced wettability studies highlight that whilst all samples differ in photo-catalytic rate, they all exhibit some form of photo-activity, as all samples start hydrophilic and upon UV irradiation at 365 nm for 24 hours they exhibit a further decrease in the water contact angle. Positions A and B unsurprisingly give the largest change in water contact angles.

Hall Effect measurements demonstrate that the left hand side of the film, which is nitrogen doped, exhibits p-type behaviour and that once niobium is found in the bulk this switches to n-type behaviour in good agreement with the literature due to the addition and population of the conduction band with electrons as a result of Nb^{5+} addition.[11,50] Thus despite niobium lying deep within the bulk it is prominent enough to define the nature of charge carrier in positions D-F. The values reported in this work compare favourably with literature reports for doped ZnO with charge carrier concentrations on the order of ~10^{20} cm^{-3} and resistivity values on the order of 10^{-3} but cannot compete with industry standards such as ITO which exhibit charge carrier concentrations and resistivity values an order of magnitude better.[51] This can be attributed in part to the inhomogeneity of the films at positions C-F, as shown in XPS, where TCO behaviour is observed.

Because the photo-activity, which is relatively surface sensitive, appears decoupled from the resistivity of the bulk at specific positions, this means that a midway point can be achieved where low concentrations of niobium are sufficient to decrease resistivity and change the nature of charge carriers whilst retaining a competitive rate of photo-catalysis imbued by nitrogen doping at positions C-D. This is because the films are relatively inhomogeneous. Thus the surface and sub-surface bulk, which exhibit little niobium but are nitrogen doped, retains a high rate of photo-catalysis whilst the bulk, which is doped with niobium, displays low resistivity values and imbues the whole material

with good TCO properties. Thus the incorporation of a high rate of photo-catalysis and good TCO properties in TiO_2 has been achieved using the combinatorial deposition regime in AACVD.

Conclusion

In conclusion, N/ Nb co-doped thin films with varying dopant concentrations have been synthesised by AACVD as a result of a combinatorial deposition regime. This allows for the rapid creation of many different samples in a single deposition. Samples were found to exhibit changes in functional properties that correlate strongly with changes in microstructure. Dopants such as nitrogen and niobium were observed to affect the physical properties of the material, creating variances in crystal structure, band gap and elemental composition. A good photo-catalytic rate, due to nitrogen doping, was observed from positions A-D whilst niobium, which was found from positions C-G deep within the bulk imbues competitive resistivity values upon the materials at these positions. Thus the crossover positions C and D therefore represent a half-way house where both photo-activity and resistivity values suitable in commercial applications are found.

This work sheds light on the interplay of TCO and photo-catalytic properties in TiO_2 based materials. We, the authors demonstrate that whilst favourable TCO and photo-catalytic properties can be imbued separately, the incorporation of both TCO and photo-catalytic properties result in a lowering in intensity of both physical phenomena. Combinatorial AACVD has also demonstrated its ability to efficiently relate variances in anion and cation co-doping to fluctuations in functional properties. This has particular importance in designing advanced functional materials for future commercialisation.

Acknowledgements

Thank you to Dr Ainara Garcia Gallastegui for useful discussions. Thank you to Pilkington NSG for the glass substrates. The project was jointly funded by the Deanship of Scientific Research (DSR), King

Abdulaziz University, Jeddah under grant no. D-1-434 and a UCL Impact scholarship. The authors therefore acknowledge the DSR and UCL with thanks for their technical and financial support.

References

1 A. J. Frank, N. Kopidakis and J. Van De Lagemaat, *Coord. Chem. Rev.*, 2004, **248**, 1165–1179.

2 A. Fujishima, T. N. Rao and D. A. Tryk, *J. Photochem. Photobiol. C*, 2000, **1**, 1–21.

3 C. Andrei, T. O'Reilly and D. Zerulla, *Phys. Chem. Chem. Phys.*, 2010, **12**, 7241–5.

4 S. H. Bossmann, C. Turro, C. Schnabel, M. R. Pokhrel, L. M. Payawan, B. Baumeister and M. Wo, 2001, 5374–5382.

5 H. Irie, Y. Watanabe and K. Hashimoto, *Chem. Lett.*, 2003, **32**, 772–773.

6 S. M. Bawaked, S. Sathasivam, D. S. Bhachu, N. Chadwick, A. Y. Obaid, S. Al-Thabaiti, S. N. Basahel, C. J. Carmalt and I. P. Parkin, *J. Mater. Chem. A*, 2014, **2**, 12849.

7 K. B. Jaimy, V. P. Safeena, S. Ghosh, N. Y. Hebalkar and K. G. K. Warrier, *Dalton Trans.*, 2012, **41**, 4824–32.

8 C. Marchiori, G. Di Liberto, G. Soliveri, L. Loconte, L. Lo Presti, D. Meroni, M. Ceotto, C. Oliva, S. Cappelli, G. Cappelletti, C. Aieta and S. Ardizzone, *J. Phys. Chem. C*, 2014, **118**, 24152–24164.

9 C. Di Valentin, E. Finazzi, G. Pacchioni, A. Selloni, S. Livraghi, M. C. Paganini and E. Giamello, *Chem. Phys.*, 2007, **339**, 44–56.

10 R. Quesada-Cabrera, C. Sotelo-Vazquez, J. A. Darr and I. P. Parkin, *Appl. Catal. B Environ.*, 2014, **160-161**, 582–588.

11 D. S. Bhachu, S. Sathasivam, G. Sankar, D. O. Scanlon, G. Cibin, C. J. Carmalt, I. P. Parkin, G. W. Watson, S. M. Bawaked, A. Y. Obaid, S. Al-Thabaiti and S. N. Basahel, *Adv. Funct. Mater.*, 2014, **24**, 5075–5085.

12 D. Kurita, S. Ohta, K. Sugiura, H. Ohta and K. Koumoto, *J. Appl. Phys.*, 2006, **100**, 096105.

13 T. Hitosugi, H. Kamisaka, K. Yamashita, H. Nogawa, Y. Furubayashi, S. Nakao, N. Yamada, A. Chikamatsu, H. Kumigashira, M. Oshima, Y. Hirose, T. Shimada and T. Hasegawa, *Appl. Phys. Express*, 2008, **1**, 1112031–1112033.

14 Y. Liu, J. M. Szeifert, J. M. Feckl, B. Mandlmeier, J. Rathousky, O. Hayden, D. Fattakhova-Rohlfing and T. Bein, *ACS Nano*, 2010, **4**, 5373–5381.

15 Y. Furubayashi, T. Hitosugi, Y. Yamamoto, K. Inaba, G. Kinoda, Y. Hirose, T. Shimada and T. Hasegawa, *Appl. Phys. Lett.*, 2005, **86**, 1–3.

16 T. Cottineau, N. Béalu, P.-A. Gross, S. N. Pronkin, N. Keller, E. R. Savinova and V. Keller, *J. Mater. Chem. A*, 2013, **1**, 2151.

17 J. Lim, P. Murugan, N. Lakshminarasimhan, J. Y. Kim, J. S. Lee, S. H. Lee and W. Choi, *J. Catal.*, 2014, **310**, 91–99.

18 A. Kafizas, C. W. Dunnill and I. P. Parkin, 2010, 8336–8349.

19 N. Noor and I. P. Parkin, *Thin Solid Films*, 2013, **532**, 26–30.

20 S. Ponja, S. Sathasivam, N. Chadwick, A. Kafizas, S. M. Bawaked, A. Y. Obaid, S. Al-Thabaiti, S. N. Basahel, I. P. Parkin and C. J. Carmalt, *J. Mater. Chem. A*, 2013, **1**, 6271.

21 C. R. Crick, J. C. Bear, P. Southern and I. P. Parkin, *J. Mater. Chem. A*, 2013, **1**, 4336.

22 P. Marchand, I. Hassan, I. P. Parkin and C. J. Carmalt, *Dalton Trans.*, 2013, **42**, 9406–22.

23 N. Chadwick, S. Sathasivam, A. Kafizas, S. M. Bawaked, A. Y. Obaid, S. Al-Thabaiti, S. N. Basahel, I. P. Parkin and C. J. Carmalt, *J. Mater. Chem. A*, 2014, **2**, 5108.

24 C. E. Knapp, A. Kafizas, I. P. Parkin and C. J. Carmalt, *J. Mater. Chem.*, 2011, **21**, 12644.

25 A. Kafizas and I. P. Parkin, *J. Am. Chem. Soc.*, 2011, **133**, 20458.

26 A. Mills, J. Wang, S.-K. Lee and M. Simonsen, *Chem. Commun. (Camb).*, 2005, 2721–3.

27 A. Ghicov, M. Yamamoto and P. Schmuki, *Angew. Chemie - Int. Ed.*, 2008, **47**, 7934–7937.

28 W. Guo, F. Zhang, C. Lin and Z. L. Wang, *Adv. Mater.*, 2012, **24**, 4761–4.

29 M. Sato, H. Hara, T. Nishide and Y. Sawada, *J. Mater. Chem.*, 1996, **6**, 1767.

30 D. Morris, Y. Dou, J. Rebane, C. Mitchell, R. Egdell, D. Law, a. Vittadini and M. Casarin, *Phys. Rev. B*, 2000, **61**, 13445–13457.

31 R. Asahi, T. Morikawa, T. Ohwaki, K. Aoki and Y. Taga, *Science*, 2001, **293**, 269–71.

32 T. Yoshida, S. Niimi, M. Yamamoto, T. Nomoto and S. Yagi, *J. Colloid Interface Sci.*, 2015, **447**, 278–81.

33 R. G. Palgrave, D. J. Payne and R. G. Egdell, *J. Mater. Chem.*, 2009, **19**, 8418.

34 M. J. Powell, C. W. Dunnill and I. P. Parkin, *J. Photochem. Photobiol. A Chem.*, 2014, **281**, 27–34.

35 F. Y. Xie, L. Gong, X. Liu, Y. T. Tao, W. H. Zhang, S. H. Chen, H. Meng and J. Chen, *J. Electron Spectros. Relat. Phenomena*, 2012, **185**, 112–118.

36 A. R. González-Elipe, R. Alvarez, J. P. Holgado, J. P. Espinos, G. Munuera and J. M. Sanz, *Appl. Surf. Sci.*, 1991, **51**, 19–26.

37 B. Jun, C. Kim, H. Kim, J. Kim and Y. Hwang, 2005, **46**, 100–103.

38 H. Tian, B. Xiao, M. Kelley, C. Reece, A. Demasi, L. Pipe and K. Smith, 2008.

39 S. Hashimoto, C. Tanaka and A. Murata, *J. Surf. Anal.*, 2006, **13**, 14–18.

40 M. Oku, H. Matsuta, K. Wagatsuma, Y. Waseda and S. Kohiki, *J. Electron Spectros. Relat. Phenomena*, 1999, **105**, 211–218.

41 S. Hashimoto and A. Tanaka, *Surf. Interface Anal.*, 2002, **34**, 262–265.

42 M. Z. Atashbar, H. T. Sun, B. Gong, W. Wlodarski and R. Lamb, *Thin Solid Films*, 1998, **326**, 238–244.

43 J. Tauc, *Mater. Res. Bull.*, 1968, **3**, 37–46.

44 A. Kafizas, C. W. Dunnill and I. P. Parkin, *J. Mater. Chem.*, 2010, **20**, 8336.

45 S. X. Zhang, D. C. Kundaliya, W. Yu, S. Dhar, S. Y. Young, L. G. Salamanca-Riba, S. B. Ogale, R.

D. Vispute and T. Venkatesan, *J. Appl. Phys.*, 2007, **102**, 013701.

46 R. Swanepoel, *J. Phys. E.*, 1983, **16**, 1214.

47 R. G. Palgrave, D. J. Payne and R. G. Egdell, *J. Mater. Chem.*, 2009, **19**, 8418.

48 T. M. Breault and B. M. Bartlett, *J. Phys. Chem. C*, 2013, **117**, 8611–8618.

49 T. M. Breault and B. M. Bartlett, *J. Phys. Chem. C*, 2012, **116**, 5986–5994.

50 Y. P. Yu, W. Liu, S. X. Wu and S. W. Li, *J. Phys. Chem. C*, 2012, **116**, 19625–19629.

51 T. Minami, *Semicond. Sci. Technol.*, 2005, **20**, S35–S44.